Influence of medium modified angular distributions and mean field on the quasielastic and inelastic peaks of neutrons induced by 1.2 GeV protons on targets with $27 \leqslant A \leqslant 232$

Khaled Abdel-Waged*

Umm Al-Qura University, Faculty of Applied Science, Physics Department, Makkah Unit 126, P.O. Box 7047, Saudi Arabia

(Received 7 February 2004; published 14 July 2004)

An analysis of the quasielastic and inelastic peaks of neutrons induced by 1.2 GeV protons on targets with $27 \leqslant A \leqslant 232$ is presented using the ultrarelativistic quantum molecular dynamics (UrQMD) model. Two distinct contributions of the nuclear medium are studied in the UrQMD framework, referred to as "in-medium" and "mean field" effects. The former only includes modifications to the *NN*-elastic and $NN \rightarrow N\Delta$ angular distributions as well as changes to the Δ-mass distribution. The latter incorporates the (QMD) interaction potential between nucleons. It is shown that in-medium effect produces an important role for enhancing the quasi-inelastic peak, while the mean field effect enhances the intensity of both peaks and becomes important in the quasielastic region. The introduction of both effects in the UrQMD calculations improves the intensity and location of the quasielastic and inelastic peaks. A rather smooth dependence of the integrated cross sections of the quasielastic and inelastic peaks on the mass number at both angles is also found and shown to be in qualitative agreement with the UrQMD incorporating these two effects.

DOI: 10.1103/PhysRevC.70.014605 PACS number(s): 25.40.Sc, 24.10.Lx, 25.40.Kv, 25.40.Ep

I. INTRODUCTION

One of the remaining open problems in the transport theoretical description of the neutron spectra at intermediate energies ($\approx$1 GeV) is the difficulty of reproducing the location and intensity of the so-called quasielastic and inelastic peaks at very forward angles [1–8]. The (quasielastic) peak, centered near the beam energy, has been interpreted as quasielastic charge exchange nucleon-nucleon (*NN*) collisions inside the target nucleus. The (quasi-inelastic) peak, located at the beam energy minus $\approx$300 MeV, is associated with the excitation of the Δ-resonance in inelastic *NN*-collisions. In contrast with the quasielastic peak, which can be attributed to a single (p,n) elastic scattering, in the quasi-inelastic region, the single (p,n) inelastic scattering contribution is superimposed to a background of multiple scattering contribution.

Over the last few years, various versions of the intranuclear cascade (INC) models have been developed to describe the neutron double differential cross sections data in the 200 MeV$-$2 GeV energy domain [2,3]. Their results, however, cannot predict the whole neutron spectra. In particular, the amplitude of the quasielastic and inelastic peaks are usually underestimated, even when a better parameterization of baryon-baryon collisions and a diffuse nuclear surface are included. Two possible origins of the observed discrepancy are the neglect of "in-medium" and/or "mean field" effects. It is shown in Ref. [3] that the in-medium cross sections do not affect the quasielastic region, as expected: since *NN*-collisions occur at the surface of the target and are energetic. This may also be true when one considers the angular distributions of the scattered *NN*-elastic collisions. On the contrary, the angular distribution involving Δ-particles in the quasi-inelastic process may be drastically changed by the medium. It has indeed been advocated that medium modified angular distribution is more important for inelastic *NN*-collisions than for elastic ones [9–11].

In order to investigate the above mentioned effects, we analyze the recent experimental data, in which both the quasielastic and inelastic peaks are prominent, with the ultrarelativistic quantum molecular dynamics (UrQMD) model [12]. The UrQMD model offers, in comparison with the INC models, two running modes: the cascade mode and the one that includes the mean field effect. The current stage (version 1.2) UrQMD code only uses free cross sections and free on-shell particles. Thus, the in-medium effect discussed here only include medium modification to the *NN*-elastic and $NN \rightarrow N\Delta$ differential cross sections as well as changes to the Δ-mass distribution. Note that, the medium modified differential cross section for *NN*-elastic scattering is already implemented in the UrQMD code.

Two points should be stressed here. First, the medium modified differential cross sections are only used, as in the UrQMD code, for the angular distributions of the two body processes but not for the corresponding total cross sections, which are taken, similar to INC models, to be free ones. Second, the above mentioned effects are studied without changing any of the standard UrQMD assumptions and using always the same default UrQMD parameters.

The organization of this paper is as follows: a brief description of the basic principles of the UrQMD model, mainly at intermediate energies, is given in Sec. II. In Sec. III predictions of both modes of UrQMD model using free space and medium modified *NN*-elastic and $NN \rightarrow N\Delta$ angular distributions are compared with one another and with the recent measurements [1] of double differential neutron production cross sections as a function of neutron kinetic energy (E_n) at 0° and 10° for $p+{}^{27}$Al, ^{56}Fe, ^{91}Zr, ^{184}W, ^{208}Pb, and ^{232}Th at 1.2 GeV. We summarize and conclude this work in Sec. IV.

*Permanent address: Physics Department, Faculty of Science, Benha University, Benha, Egypt. Email address: khelwagd@yahoo.com

II. DESCRIPTION OF THE UrQMD MODEL

The details of the UrQMD formalism have been explained in Ref. [12]. We will only comment on those points which are important for understanding of the calculation discussed in Sec. III.

Nuclear collisions are assumed to be described by the sum of independent binary hadron-hadron (hh) collisions. Each hh collision is assumed to take place at the distance of closest approach, that is, two particles collide if their distance d_{trans} fulfills the relation:

$$d_{trans} \leqslant \sqrt{\frac{\sigma_{\rm tot}}{\pi}}, \quad \sigma_{\rm tot} = \sigma(\sqrt{s}, \text{type}). \tag{1}$$

The total cross section $\sigma_{\rm tot}$ depends on the center-of-mass (c.m.) energy ($\sqrt{s}$) and on the species and quantum number of the incoming particles, d_{trans} is defined as the covariant relative distance between the two particles:

$$d_{trans} = \sqrt{(\boldsymbol{r}_1 - \boldsymbol{r}_2)^2 - \frac{(\boldsymbol{r}_1 - \boldsymbol{r}_2)\cdot(\boldsymbol{p}_1 - \boldsymbol{p}_2)}{(\boldsymbol{p}_1 - \boldsymbol{p}_2)^2}} \tag{2}$$

with $\boldsymbol{r}_i$ being the location and $\boldsymbol{p}_i$ the momentum in the rest frame of the colliding particles.

The inelastic hh collisions produce resonances at low and intermediate energies, while at high energies ($\sqrt{s}=5$ GeV for baryon-baryon and 3 GeV for meson-baryon and meson-meson reactions) color strings are formed and they decay into hadrons according to the Lund string model [13]. There are 55 baryon and 32 meson states as discrete degrees of freedom in the model as well as their antiparticles and explicit isospin projected states with masses up to 2.25 GeV/c^2. All of these hadronic states can propagate and reinteract in phase space.

The UrQMD uses a table-look-up for the total and elastic proton-proton and proton-neutron cross sections. The details of other hh-cross sections implemented in the UrQMD model at intermediate energies are given in Appendix A.

Except the medium modified differential cross sections for NN-elastic scattering, the UrQMD model does not include any medium effects such as in-medium cross sections and in-medium masses.

On the basis of quantum molecular dynamics, potential interactions are enforced for the scattered nucleons. The single particle wave function of each nucleon is represented by a Gaussian wave packet, having the phase-space centroid parameters of $\boldsymbol{R}_i$ and $\boldsymbol{P}_i$ for the ith nucleon. The total wave function is assumed to be a product wave function of nucleon Gaussian wave packet. The equation of motion for their centroids ($\boldsymbol{R}_i$ and $\boldsymbol{P}_i$) is given by

$$\frac{dR_j}{dt} = \frac{\partial H}{\partial P_j}, \quad \frac{dP_j}{dt} = -\frac{\partial H}{\partial R_j}. \tag{3}$$

The Hamiltonian H consists of the kinetic energy and the effective interaction energy,

$$H = T + V,$$

$$T = \sum_j [(p_j^2 + m_j^2)^{1/2} - m_j],$$

$$V = V_{\rm Skyrme} + V_{\rm Yukawa} + V_{\rm Coulomb} + V_{\rm Pauli}. \tag{4}$$

In this interaction energy, the following terms are included: Skyrme-type density dependent interaction ($V_{\rm Skyrme}$), Yukawa potential ($V_{\rm Yukawa}$), Coulomb potential between protons ($V_{\rm Coulomb}$), and the Pauli potential ($V_{\rm Pauli}$). The form of each term is given by

$$V_{\rm Skyrme} = \frac{t_1}{2\rho_0}\sum_{i=1}^{A}\sum_{\substack{k=1\\k\neq i}}^{A}\tilde{\rho}_{ik} + \frac{t_\gamma}{(\gamma+1)\rho_0^\gamma}\sum_{i=1}^{A}\left(\sum_{\substack{k=1\\k\neq i}}^{A}\tilde{\rho}_{ik}\right)^\gamma,$$

$$V_{\rm Yukawa} = \frac{V_0^{\rm Yuk}}{2}\sum_{i=1}^{A}\sum_{\substack{k=1\\k\neq i}}^{A}\frac{1}{2\boldsymbol{r}_{ik}}\exp\left(\frac{1}{4\alpha\gamma_Y^2}\right) \times\left\{e^{-\boldsymbol{r}_{ik}/\gamma_Y}\left[1-\text{erf}\left(\frac{1}{2\gamma_Y\sqrt{\alpha}}-\sqrt{\alpha}\boldsymbol{r}_{ik}\right)\right] - e^{\boldsymbol{r}_{ik}/\gamma_Y}\left[1-\text{erf}\left(\frac{1}{2\gamma_Y\sqrt{\alpha}}+\sqrt{\alpha}\boldsymbol{r}_{ik}\right)\right]\right\},$$

$$V_{\rm Coulomb} = \frac{1}{2}e^2\sum_{i=1}^{A}\sum_{\substack{j=1\\j\neq i}}^{A}\frac{1}{r_{ij}}\text{erf}(\sqrt{\alpha}r_{ij}),$$

$$V_{\rm Pauli} = \frac{1}{2}V_0^P\left(\frac{\hbar}{p_0 q_0}\right)^3\left(1+\frac{1}{2\alpha q_0^2}\right)^{-3/2} \times\sum_{i=1}^{A}\sum_{\substack{k=1\\k\neq i}}^{A}\exp\left(\frac{-\alpha r_{ik}^2}{2\alpha q_0^2+1}-\frac{p_{ik}^2}{2p_0^2}\right)\delta_{\tau_i\tau_k}\delta_{\xi_i\xi_k}, \tag{5}$$

where $\boldsymbol{r}_{ik}=\boldsymbol{R}_i-\boldsymbol{R}_k$, $\boldsymbol{p}_{ik}=\boldsymbol{P}_i-\boldsymbol{P}_k$, τ_i and ξ_i denote the spin-isospin index of nucleon (i), and the "interaction density" $\tilde{\rho}_{ik}=(\alpha/\pi)^{3/2}e^{-\alpha(\boldsymbol{R}_i-\boldsymbol{R}_k)^2}$.

The summation runs over all projectile and target nucleons, $\rho_0=0.168$ fm^{-3} is the normal nuclear density, and erf denotes the error function. The values of the parameters appearing in Eq. (5) are chosen to be [12], $\alpha=0.1152$ fm^{-2}, $t_1=-84.5$ MeV fm^3, $\gamma=1.46$, $t_\gamma=188.2$ MeV fm^6, $V_0^{\rm Yuk}=-85.1$ MeV fm, $\gamma_Y=1.0$ fm, $V_0^{\rm Paul}=99.5$ MeV, $q_0=3$ fm, and finally, $p_0=120$ MeV/c, which corresponds to the hard equation of states.

In the UrQMD model, the ground state configuration is obtained by the following packing procedure. The centroids of the Gaussians $\boldsymbol{R}_i$ are randomly distributed within a sphere with radius,

$$R = 1.124\left[\tfrac{1}{2}(A + (A^{1/3} - 1)^3)\right]^{1/3}, \tag{6}$$

where A is the mass number of the nucleus. In choosing $\boldsymbol{R}_i$ a minimum distance of 1.6 fm is imposed between identical nucleons and 1.0 fm for the others. The initial momenta of the nucleons are randomly chosen between zero and the local Thomas-Fermi momentum: $p_F^{\max} = \hbar c(3\pi^2\rho)^{1/3}$, with ρ being the corresponding local-proton or neutron density. The phase space density at the location of each nucleon is evaluated: if the phase space density is too high, then the location of that nucleon is rejected and a new location is randomly chosen. This procedure reduces fluctuations in the mean density of the nucleus.

The UrQMD calculation is carried out up to a time scale referred to as the transition time $t_{\rm tr}$. We have selected $t_{\rm tr}$ to be 100 fm/c, because this value was enough to obtain stable neutron spectra from the (p,xn) reaction against a change of $t_{\rm tr}$ as shown in Ref. [14]. At $t_{\rm tr}$=100 fm/c, the position of each nucleon is used to calculate the distribution of mass and charge numbers (referred to as "prefragments"). In determining the mass and charge numbers of the prefragments, the minimum spanning tree method [15] is employed. The prefragments thus identified are then Lorentz boosted into their rest frames to evaluate their excitation energies. When the prefragment is in the excited state, the statistical decay via $n,p,d,t,{}^3$He, and α emissions is considered based on the Weisskopf approximation [16].

In the numerical calculations, the UrQMD (version 1.2) is run in two modes, the cascade mode (UrQMD/C) and the one that includes the mean field effect (UrQMD/M).

In addition, the UrQMD predictions are compared using free space and medium modified differential cross sections for NN-elastic and $NN \rightarrow N\Delta$ processes. The used differential cross sections expressions are given in Appendix B. It is worth stressing again that the medium modified differential cross sections are used to determine the scattering angles between the outgoing particles in elementary hh collisions but not for the corresponding total cross sections.

As will be discussed in Sec. III it is not enough to define the medium modified differential cross section for the $NN \rightarrow N\Delta$ reaction but we also need to use an appropriate mass distribution for the Δ-resonance, $\langle m_\Delta \rangle$. We choose [17]

$$\langle m_\Delta \rangle = \frac{\int_{m_N+m_\pi}^{\sqrt{s}-m_N} f(m_\Delta) m_\Delta dm_\Delta}{\int_{m_N+m_\pi}^{\sqrt{s}-m_N} f(m_\Delta) dm_\Delta}, \tag{7}$$

where

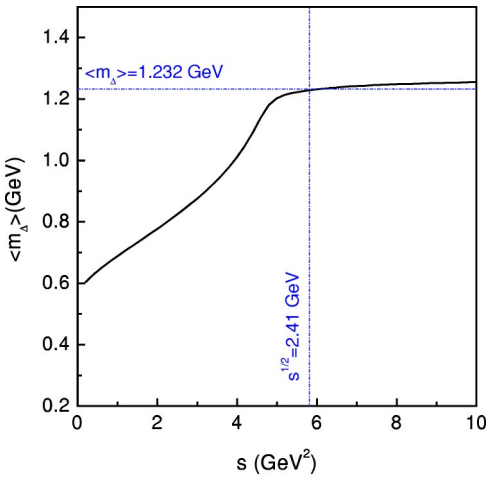

FIG. 1. (Color online) The delta mass distribution $\langle m_\Delta \rangle$ as a function of the total energy of a two particle system in free space (s).

$$f(m_\Delta) = \frac{1}{\pi}\frac{\Gamma_0/2}{(\Gamma_0/2)^2 + (m_\Delta - 1232)}. \tag{8}$$

Inserting Eq. (8) into Eq. (7) one can obtain,

$$\langle m_\Delta \rangle = 1232 + (\arctan Z_+ - \arctan Z_-)^{-1}\frac{\Gamma_0}{4}\ln\left[\frac{1+Z_+^2}{1+Z_-^2}\right], \tag{9}$$

where

$$Z_+ = (\sqrt{s} - m_N - 1232)(2/\Gamma_0),$$

$$Z_- = (m_N + m_\pi - 1232)(2/\Gamma_0),$$

with Γ_0=110 MeV. It is shown in Ref. [17] that a successful reproduction of the empirical free NN-inelastic cross section can be realized using the mass distribution of Eq. (9). The dependence of $\langle m_\Delta \rangle$ on s is depicted in Fig. 1. One can find that, as the total energy s increases the $\langle m_\Delta \rangle$ increases so rapidly up to a kinetic energy 1.2 GeV ($\sqrt{s} \approx 2.41$ GeV). After reaching the resonance mass $\langle m_\Delta \rangle$=1232 MeV, the $\langle m_\Delta \rangle$ increases very slowly with the increasing of s.

In what follows we denote the improvements established using the medium modified NN-elastic and $NN \rightarrow N\Delta$ differential cross sections as well as changes to the Δ-mass distribution in the UrQMD/C and UrQMC/M as "UrQMD/CM" and "UrQMD/MM," respectively. In this work, the default UrQMD parameters are selected, and no adjustment is attempted.

III. RESULTS AND DISCUSSION

In this section, we display the predictions of the UrQMD model (coupled with free and medium modified differential cross sections) along with the recent measurements [1] of double differential neutron production cross sections as a function of neutron kinetic energy (E_n) at 0° and 10° for p + ^{27}Al, ^{56}Fe, ^{91}Zr, ^{184}W, ^{208}Pb, and ^{232}Th at 1.2 GeV, in

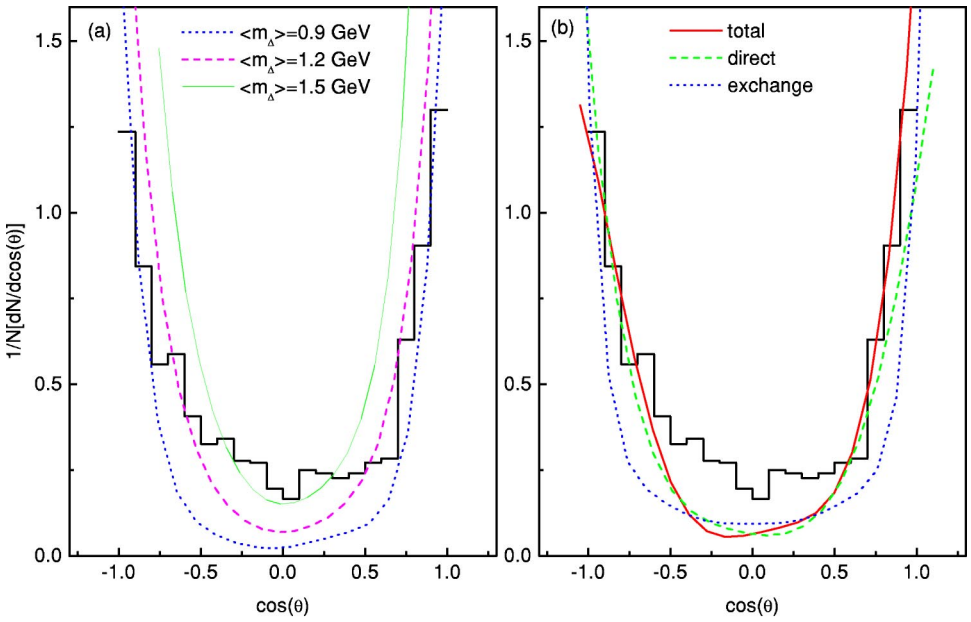

FIG. 2. (Color online) The angular distribution of the neutron calculated using Eq. (B9) for the reaction $p+p \rightarrow n+\Delta^{++} \rightarrow n+p+\pi^+$ at 0.97 GeV. (a) Shows the calculations with different delta mass distributions. (b) The contributions of the direct and exchange terms. The solid histograms show the data from Ref. [19].

which both the quasielastic and inelastic peaks are prominent. A full comparison between the UrQMD calculations, without the $NN \rightarrow N\Delta$ medium modified differential cross sections, and the data at various angles can be found in Ref. [14] for $p+{}^{27}$Al, ^{56}Fe, and ^{91}Zr at 1.2 GeV.

The measured energy spectra (see Figs. 3 and 5) are characterized by a narrow peak at a kinetic energy near that of the beam energy and at lower energy a broad peak centered around 873 MeV and 760 MeV at 0° and 10°, respectively. The upper peak (denoted as "quasielastic peak") is due to a single (p,n) elastic scattering in the forward direction and shifted toward large energy losses compared to the quasi-free kinematics, by 20–30 MeV, more or less independently of the target mass. The lower peak (denoted as "quasi-inelastic peak") is about 400 MeV wide and is thought to be due to Δ-resonance excitation: $NN \rightarrow N\Delta$ (a single (p,n) inelastic scattering with multiple scattering contributions). Below we are going to investigate these two peaks by employing the UrQMD model with different (free and medium modified) angular distributions. We performed 20000 simulations at various impact parameters from 0 to $R+0.5$ fm, where R is the target radius given by Eq. (6). In order to have sufficient statistics, calculations were done for angular bins of 3.5 and 5 at 0° and 10°, respectively.

The error bars in Figs. 3 and 5 include statistical uncertainty only [1]. The thickness of the targets also induces some distortion in the neutron double differential spectra. The effect of the target thickness on the neutron spectra results in a depopulation of the intermediate energy part of the spectra (between 200 and 600 MeV) and a 30 MeV downward shift of the location of the quasielastic peak [1]. Calculations using LAHET high energy transport code system [18] were performed in Ref. [1] for targets with actual geometry and an infinitely thin one in order to assess the order of magnitude of the depopulation. It is shown that the difference is very small for the Pb target and becomes larger as both the target mass number and angle decrease. The UrQMD predictions shown here do not include these corrections.

Let us first check the validity of Eq. (B9) for binary collision $NN \rightarrow N\Delta$. Figure 2 displays the angular distribution of the neutron calculated using Eq. (B9) for the reaction $pp \rightarrow np\pi^+$ at $E_{\mathrm{lab}}=0.97$ GeV as compared with experiment [19]. Note that 90% of this reaction goes through $pp \rightarrow n+\Delta^{++} \rightarrow n+p+\pi^+$ and only 10% through $pp \rightarrow p+\Delta^+ \rightarrow p+n+\pi^+$. The results of Eq. (B9) are displayed in Fig. 2(a) for different values of $\langle m_\Delta \rangle$. When $\langle m_\Delta \rangle = m_N + m_\pi$ the best fit to the experimental data can be obtained [see Fig. 2(b)]. The contributions of the direct term, Eq. (B10), and the exchange term, Eq. (B11), are also shown in Fig. 2(b). One can easily find that the observed neutron angular distribution can be reached if only the exchange term is taken into account. The underestimation of the observed angular distribution around $\theta=90°$ is of no importance as far as the numerical simulations are concerned.

In Fig. 3 we plot the double differential cross sections of the neutron as a function of E_n at 0° (left panels) and 10° (right panels) for the reactions under study. The solid circles with error bars represent the experimental data. The histograms denote the results of the UrQMD/C. In the same figure, we plot the results of UrQMD/C with different choices of $\langle m_\Delta \rangle$. The dotted histograms are the results obtained with $\langle m_\Delta \rangle = m_N + m_\pi$, while the bold solid histograms are those with the simulated mass distribution of Eq. (9). The former case corresponds to neutrons following the quasi-free pion production from reactions like $pn \rightarrow pn\pi^\circ$, $pn \rightarrow nn\pi^+$, and $pp \rightarrow np\pi^+$, and the latter to the Δ-resonance excitation; $NN \rightarrow N\Delta$. As one can see the quasi-inelastic peaks at 0° and 10° are predominately determined by the mass distribution of the Δ-resonance.

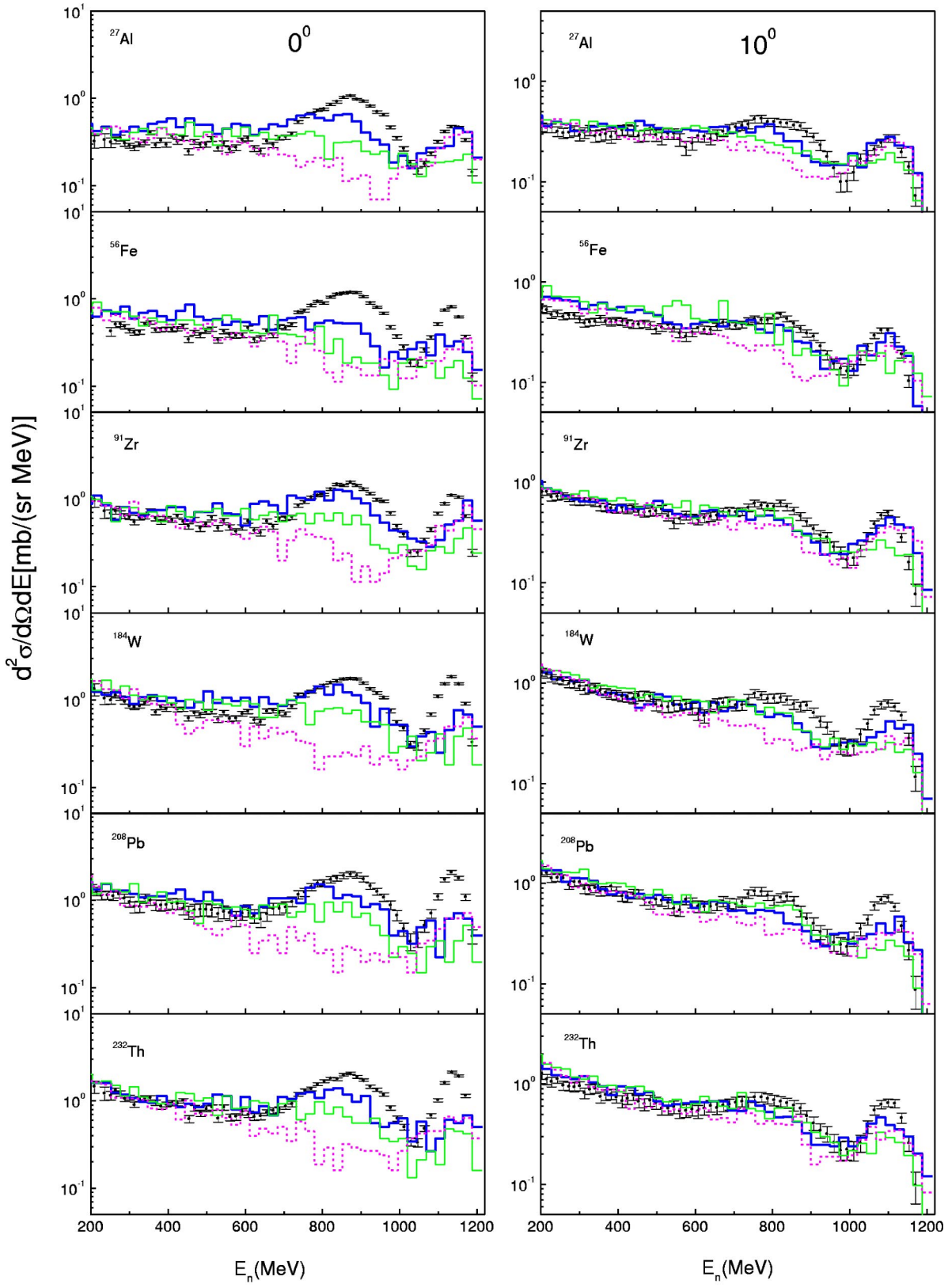

FIG. 3. (Color online) Neutron energy spectra at 0° (left panels) and 10° (right panels) from 1.2 GeV proton interactions with targets of (from the bottom): ^{232}Th, ^{208}Pb, ^{184}W, ^{91}Zr, ^{56}Fe, and ^{27}Al. The bold solid histograms denote the UrQMD/C calculations with the simulated mass distribution of Eq. (9), while the dotted histograms are those with $\langle m_\Delta \rangle = m_N + m_\pi$. The thin solid histograms represent the UrQMD/C calculations with free parametrizations. The experimental data (solid circles with error bars) are taken from Ref. [1].

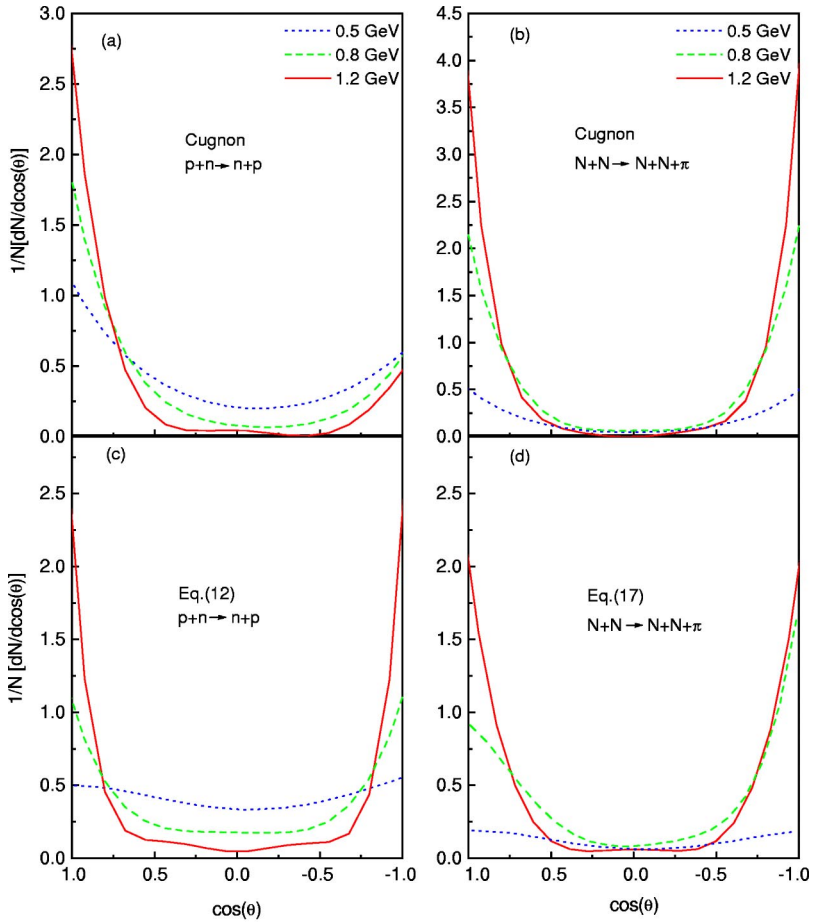

FIG. 4. (Color online) The predicted angular distributions of neutrons evaluated at different laboratory energies for $p+n \rightarrow p+n$ (left panels) and $N+N \rightarrow N+N+\pi$ (right panels). (a) and (b) are the results calculated by the free Cugnon parametrizations, Eqs. (B1)–(B3), while (c) and (d) are those calculated by Eqs. (B4) and (B9), respectively.

The quasielastic peaks at 0° are underestimated by the UrQMD/C calculations [using the centroid mass of Eq. (9)] for the reactions under study, although they are better reproduced for $p+^{27}$Al and ^{91}Zr. In contrast, the intensity of the quasielastic peaks are reproduced at 10°, but some discrepancy still remains as the mass number of the target increases.

Let us next investigate the influence of in-medium correction on the quasielastic and inelastic peaks for the reactions under study. The in-medium correction is defined by the difference between the observables for medium modified differential cross sections, Eqs. (B4) and (B9), and for free ones, Eqs. (B1)–(B3), in the nuclear medium. For the latter case we use the same parametrizations presented in Ref. [20], with which a successful reproduction of the empirical free *NN*-differential cross sections are obtained. The predicted differential cross sections at several energies for $pn \rightarrow pn$ and $NN \rightarrow NN\pi$ are displayed in Figs. 4. We see that, although the angular distributions for free parametrizations are more forward peaked (cf. Figs. 4), the UrQMD/C calculations in conjunction with the medium modified parametrizations lead to an enhancement of the quasi-inelastic (at 0°) and elastic (at 10°) peaks (see Fig. 3). On the other hand, the quasi-inelastic peaks at 10° are rather insensitive to different parametrizations.

In order to study the influence of the mean field on the quasielastic and inelastic peaks, we compare in Fig. 5 both the UrQMD/CM and UrQMD/MM results with the experimental data for the reactions under study. We found that the mean field effect is most dramatic in the quasielastic region whereas it is less dramatic in the quasi-inelastic region. Both the intensity and the location of the quasielastic peaks at 0° are now better reproduced by the UrQMD/MM calculations. For the location, we neglected the 30 MeV downward shift of the peak location, which arises from the thickness of the target: Taking into account this shift would yield an even better agreement with the data. In contrast, at 10° the quasielastic peaks are getting broader in comparison to the data with increasing the mass number of the target nucleus. On the other hand, the broadening of the quasi-inelastic peaks is satisfactorily reproduced by the UrQMD/MM calculations at 0° and 10°, except for $p+^{27}$Al and ^{56}Fe reactions.

From Fig. 5 one notices that the neutron spectra below the quasi-inelastic peak are overestimated by the UrQMD/MM calculations for $27 \leqslant A \leqslant 184$ at 0°, and to a lesser extent at 10°. Part of the overestimation may be due to the neglect of the finite thickness of the target by the UrQMD/MM calculations. For the Pb target, where the thickness of the target is reported to be very small [1], the agreement is shown to be quite satisfactory.

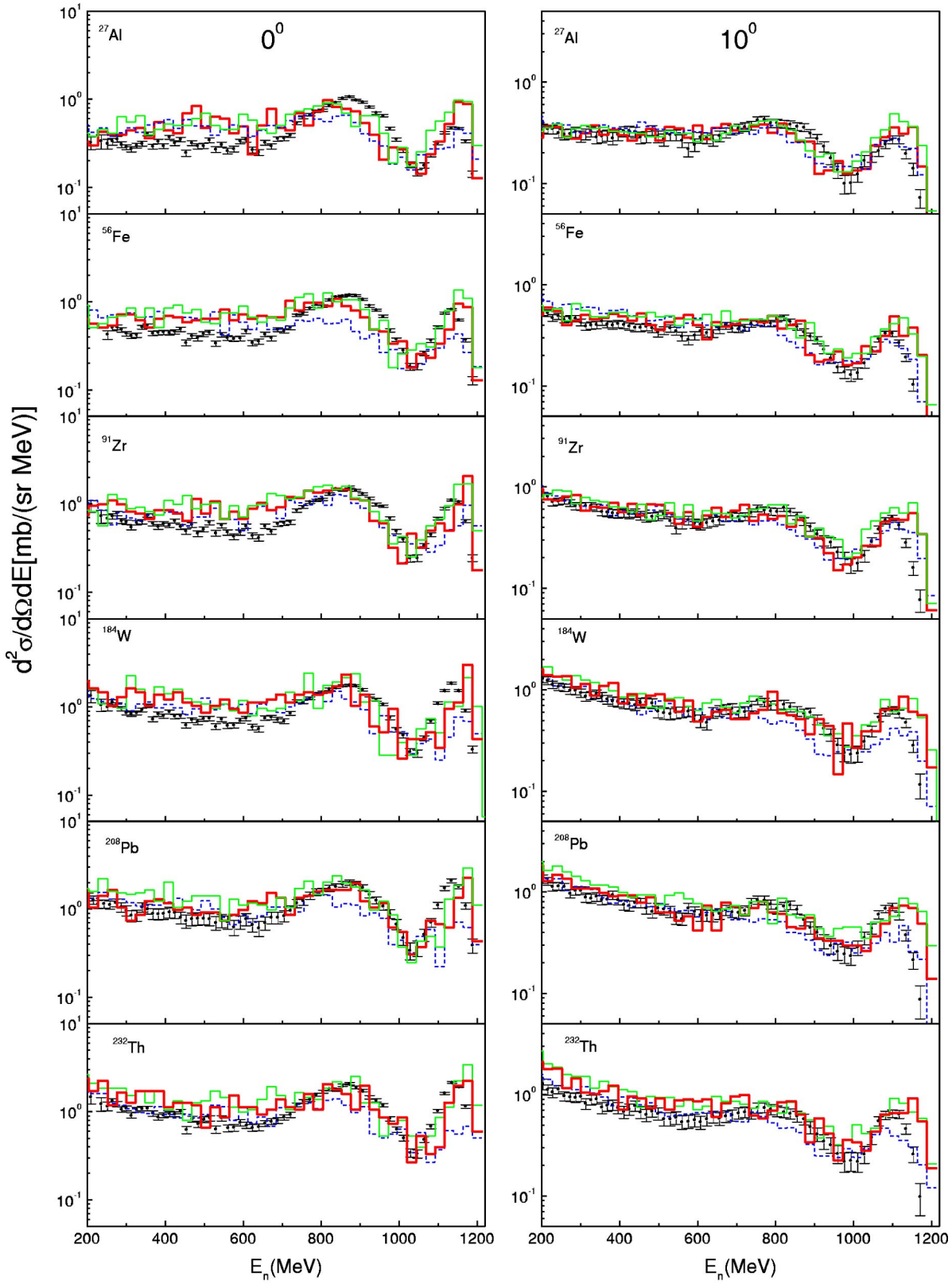

FIG. 5. (Color online) Same as Fig. 3, but here the bold solid and small dashed histograms denote the UrQMD/MM and UrQMD/CM calculations, respectively. The thin solid histograms denote the UrQMD/MM calculations that includes the $N+\Delta \rightarrow N+N$ process.

In Ref. [3] using the INC model, several effects are used to investigate the quasielastic and inelastic peaks for $p+^{208}$Pb at 800 MeV. These effects include in-medium cross sections, refraction at the nuclear surface, stopping time, Pauli blocking and a diffuse nuclear surface. In all the effects studied, the only one which increase the intensity of the

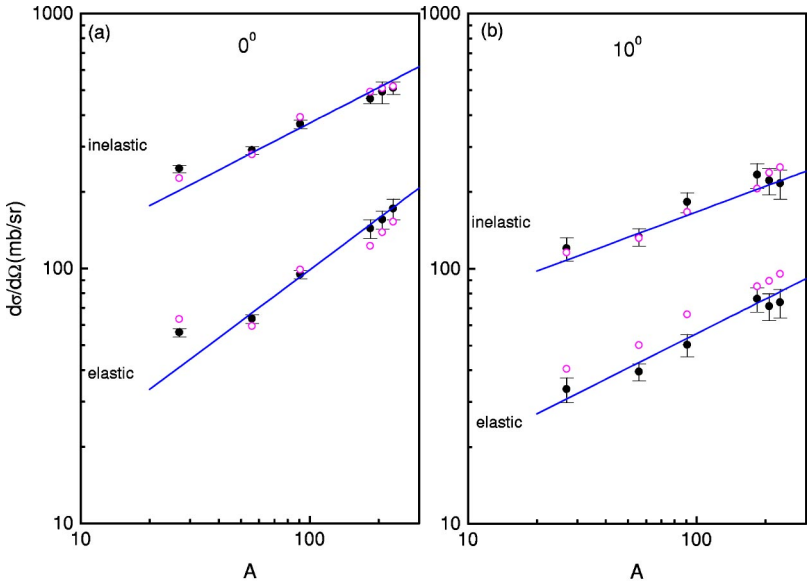

FIG. 6. (Color online) Plot of the cross sections integrals $[\int(d^2\sigma/d\Omega dE)dE]$ at 0° (left panels) and 10°(right panels) of the quasielastic and inelastic associated regions of the neutron spectra versus the mass number of the target. Solid circles with error bars represent results extracted from experimental data shown in Figs. 3 and 5. The solid lines give the results of the power law fits to the present data (solid circles with error bars) for the two regions at both angles. Results of the UrQMD/MM calculation of the quasielastic and inelastic cross sections for each nucleus are plotted as open circles.

quasielastic and inelastic peaks is the introduction of a diffuse nuclear surface. Recently [2], a new version of the INC model (INCL4) is proposed, which accommodate a diffuse nuclear surface, for the description of the reactions under study. It is shown that the width of the quasielastic and inelastic peaks are underestimated by a factor of 2 or so. This may suggest that it is very important to take into account the mean field as well as the medium modified $NN \rightarrow NN$ and $NN \rightarrow N\Delta$ differential cross sections for the description of the quasielastic and inelastic peaks in proton induced reactions.

In Fig. 5, we additionally investigate the influence of the reverse process $N\Delta \rightarrow NN$ on the quasi-inelastic and elastic peaks for the reactions under study. It is assumed, as in Ref. [9], that the angular distributions of $N\Delta \rightarrow NN$ and $NN \rightarrow N\Delta$ are similar. We show that the implementation of this channel in the UrQMD/MM calculation improves the intensity of both the quasi-inelastic (at 0° and 10°) and elastic (at 0°) peaks (see thin histograms in Fig. 5) but leads to a broadening of the quasielastic peaks, especially at 10°. This also indicates that the delta degrees of freedom survive in the nuclear medium.

Finally, in order to ascertain any systematic trends as a function of the target mass that may be present in the data and the calculation, the cross section for the quasielastic and inelastic peaks were integrated over energy. The energy values used to divide the two regions for 0° and 10° were arbitrarily taken to be 1068 and 1011 MeV, respectively. The integrals over the two regions for the six targets as a function of the mass number are shown in Fig. 6. The rather smooth dependence on the mass number of the two cross sections for both angles led us to attempt a fit of the form $d\sigma/d\Omega = \alpha A^{\beta}$. The values of the parameters extracted from the data are given in Table I and the fits are plotted in Fig. 6. At 0°, the cross section for the quasielastic region is seen to vary as $A^{2/3}$, whereas the quasi-inelastic region vary as $A^{1/2}$. The corresponding values at 10° are $A^{1/2}$ and $A^{1/3}$, respectively.

Previous measurements [21] at 800 MeV protons on targets with $27 \leqslant A \leqslant 238$ have indicated that integral neutron yields in the quasielastic region at 0° vary as $A^{2/3}$, in qualitative agreement with the present results.

The integrated cross section for each nucleus has been calculated by the UrQMD/MM, that includes only the $NN \rightarrow NN$ and $NN \rightarrow N\Delta$ processes. The results of this calculation are plotted as open circles in Fig. 6. As one can see, the overlap with the data is quite good and in qualitative agreement with the trend of the measured cross sections, except at 10° in the quasielastic region.

It should be mentioned that the integrated cross sections of the quasielastic peaks at 0° for 800 MeV protons on targets with $27 \leqslant A \leqslant 238$ are poorly determined by a single scattering model based on Glauber approach [21].

IV. SUMMARY AND CONCLUSIONS

Two distinct contributions of the nuclear medium are investigated in the UrQMD framework, referred to as "in-

TABLE I. Values of parameters extracted from power law fit: αA^{β}.

Region	α	β
At 0°		
quasielastic	4.49	0.671
Quasi-inelastic	44.0	0.463
At 10°		
quasielastic	7.00	0.450
Quasi-inelastic	36.0	0.333

medium" and "mean field" effects. The former includes modification to the *NN*-elastic and $NN \rightarrow N\Delta$ angular distributions as well as changes to the Δ-mass distribution. The latter incorporates interaction potential between nucleons. The in-medium effect is defined as the difference between the observables for the medium modified angular distributions and for free ones. The mean field effect is given as the difference between the UrQMD/MM and UrQMD/CM on the observables, that is when the two running UrQMD modes are supplemented with the medium modified angular distributions as well as changes to the Δ-mass distribution.

The influence of these two effects on the quasielastic and inelastic peaks of neutrons at 0°and 10° are studied for $p + {}^{27}$Al, ^{56}Fe, ^{91}Zr, ^{184}W, ^{208}Pb, and ^{232}Th at 1.2 GeV. From the calculation results we can get the following conclusions:

(1) The quasi-inelastic peak is predominately determined by the mass distribution of the intermediate excited delta resonance: The delta degrees of freedom survive in the nuclear medium.

(2) The in-medium effect plays an important role for enhancing the quasi-inelastic peak.

(3) The mean field effect enhances both peaks and becomes important in the quasielastic region.

(4) A better reproduction of the two peaks is obtained with UrQMD/MM than with UrQMD/C using free angular distributions.

(5) Including the $N\Delta \rightarrow NN$ process in the UrQMD/MM calculations improves the description of the quasi-inelastic peak.

(6) The neutron spectra below the quasi-inelastic peak are satisfactorily reproduced by the UrQMD/MM when the effect of target thickness plays a minor role.

(7) The integrated cross sections for the quasielastic and inelastic peaks at both angles show a smooth dependence on the mass number of the six targets, and are well reproduced by the UrQMD/MM calculations.

Thus, the quality of the results presented here and elsewhere [14] (see Refs. [2,3] for a comparison) induces us to believe that the UrQMD approach is much more appropriate for taking proper account of the collision process. However, further possible improvements of the UrQMD model at intermediate energies are still needed. These include the following:

(i) As we do for the angular distributions, one should use medium modified cross sections for $NN \rightarrow NN$ and $NN \rightarrow N\Delta$ processes.

(ii) Besides the inclusion of the delta in the collision part and in the delta mass distribution it also has to be included in the mean field part of the theory.

(iii) More realistic spatial and momentum densities should be used instead of the crude box approximation.

(iv) A self-consistent minimization of the energy of the initial nuclei should be implemented instead of the normal packing procedure.

ACKNOWLEDGMENTS

It is a pleasure to thank the UrQMD collaborators, in particular Dr. H. Weber, for making the URQMD code (version 1.2) available to us. We are also grateful to Professor S. Leray for providing us with the raw data presented here.

APPENDIX A

For the convenience of the reader, we give in this Appendix the most important *hh*-cross sections implemented in the UrQMD model.

At 1.2 GeV incident energy ($\sqrt{s}=2.41$ GeV) the most important *hh* reaction channels, included in the collision term of Eq. (1), are

$$\begin{aligned}
&(1)\ B_i + B_j \rightarrow B_i + B_j;\\
&(2)\ N + N \rightarrow N + \Delta_{1232};\\
&(3)\ N + \Delta_{1232} \rightarrow N + N;\\
&(4)\ N + N \rightarrow N + \Delta^*;\\
&(5)\ N + N \rightarrow \Delta_{1232} + N^*;\\
&(6)\ N + N \rightarrow N + N^*;\\
&(7)\ N + N^* \rightarrow N + N;\\
&(8)\ N + \pi \rightarrow \Delta_{1232};\\
&(9)\ N + \pi \rightarrow N^*;\\
&(10)\ \Delta_{1232} + \pi \rightarrow N^*;
\end{aligned} \tag{A1}$$

where B denotes a baryon, and N, more specifically, a nucleon. The Δ_{1232} is explicitly listed, whereas higher excitations of the Δ-resonance have been denoted as Δ^*.

For the production of baryonic resonances [channels 2, 4, 5, and 6 in Eq. (A1)] the cross sections are parameterized according to the general form,

$$\sigma_{1,2\rightarrow 3,4}(\sqrt{s}) \propto (2S_3+1)(2S_4+1)\frac{p_{3,4}}{p_{1,2}}\frac{1}{s}|M(m_3,m_4)|^2, \tag{A2}$$

where $S_i, i=3,4$ express the spin of the particles in the final state and $p_{i,j}$ corresponds to the c.m. momentum of the particles (i) and (j). Specific assumptions are made with regard to the form of the matrix element $|M(m_3,m_4)|^2$ for each resonance production channel. For channel 2 in Eq. (A1),

$$|M(m_3,m_4)|^2 = A\frac{m_\Delta^2\Gamma_\Delta^2}{((\sqrt{s})^2-m_\Delta^2)^2+m_\Delta^2\Gamma_\Delta^2}, \tag{A3}$$

is used with $m_\Delta=1232$ MeV, $\Gamma_\Delta=115$ MeV, and $A=40000$. As for the channels 4, 5, and 6 in Eq. (A1),

$$|M(m_3,m_4)|^2 = A\frac{1}{(m_4-m_3)^2(m_4-m_3)^2}, \tag{A4}$$

is taken with $A=6.3$ for channel 6, $A=12$ for the channel 4, and $A=3.5$ for channel 5. The free parameters in Eqs. (A3)

and (A4) are tuned to experimental measurements.

The cross sections for channels 3 and 7 in Eq. (A1) are determined by the law of detailed balance from the cross sections of channels 2 and 6, respectively,

$$\sigma_{3,4\to1,2} \propto \frac{\langle p_{1,2}^2\rangle}{\langle p_{3,4}^2\rangle}\frac{(2S_1+1)(2S_2+1)}{(2S_3+1)(2S_4+1)}\sigma_{1,2\to3,4}. \quad \text{(A5)}$$

The integration over the mass distributions of the resonances in Eq. (A5) has been denoted by the brackets $\langle\rangle$, e.g.,

$$\langle p_{3,4}^2\rangle = \int\int p_{3,4}^2(\sqrt{s},m_3,m_4)A_3(m_3)A_4(m_4)dm_3dm_4. \quad \text{(A6)}$$

The mass distribution $A_r(m)$ in Eq. (A6) is given by the Breit-Wigner distribution with a mass dependent width,

$$A_r(m) = \frac{1}{N}\frac{\Gamma(m)}{(m_r-m)^2+\Gamma(m)^2/4}, \quad \text{(A7)}$$

where N denotes the normalization constant.

In the case of π-absorption on baryons (channels 8, 9, and 10), the total meson-baryon cross section is given by

$$\sigma(MB\to R) = \sum_{R=\Delta,N^*}|C(MB,R|^2\frac{(2S_R+1)}{(2S_M+1)(2S_B+1)}\frac{\pi}{p_{\text{C.M.}}^2} \times\frac{\Gamma_{R\to MB}\Gamma_{\text{tot}}}{(\sqrt{s}-m_R)^2+\Gamma_{\text{tot}}^2/4}, \quad \text{(A8)}$$

where $C(MB,R)$ are the Clebsch-Gordon coefficients. S_R, S_B, and S_M denote the spin of the resonance, the decaying baryon and meson, respectively. The full width Γ_{tot} is a sum of all partial decay width $\Gamma_{R\to MB}$ for resonance R into mesons M and baryons B, which depends on the momentum of the decaying particle,

$$\Gamma_{R\to MB} = \Gamma_{R\to MB}^0\frac{m_R}{m}\left(\frac{p_{\text{C.M.}}(m)}{p_{\text{C.M.}}(m_R)}\right)^{2l+1}\frac{1.2}{1+0.2\left(\frac{p_{\text{C.M.}}(m)}{p_{\text{C.M.}}(m_R)}\right)^{2l+1}}, \quad \text{(A9)}$$

$\Gamma_{R\to MB}^0$ is the partial decay width of the resonance into the channel M and B. l and $p_{\text{C.M.}}(m)$ are the relative angular momentum and the relative momentum in their rest frame, respectively.

The decay of the resonances proceeds according to the branching ratios compiled by the particle data group [22]. The resonance decay products have isotropical distributions in the rest frame of the resonance.

APPENDIX B

In this appendix we give the expressions of the free space and medium modified NN-elastic and $NN\to N\Delta$ differential cross sections used in this paper.

1. Free space differential cross sections

(1) pp-elastic scattering [23]:

$$\frac{d\sigma_{pp}}{dt} \approx e^{-A(s)t}, \quad \text{(B1)}$$

where

$$A(s) = 6\frac{(3.65(\sqrt{s}-1.8766))^6}{1+(3.65(\sqrt{s}-1.8766))^6}.$$

(2) pn-elastic scattering [20]:

$$\frac{d\sigma_{pn}}{dt} \approx (e^{B_{pn}t}+\alpha\, e^{B_{pn}u}), \quad \text{(B2)}$$

where t and u are the Mandelstam variables. The coefficients B_{pn} and α are given by

$$B_{pn} = 3.68 + 0.76p_{\text{lab}},$$

$$\alpha = (0.8/p_{\text{lab}}),$$

where p_{lab} is the incident laboratory momentum in GeV.

(3) $NN\to N\Delta$ [20]:

$$\frac{d\sigma_{NN\to N\Delta}}{dt} \approx (e^{B_{in}t}+e^{-B_{in}t}), \quad \text{(B3)}$$

with

$$B_{in} = 5.287\left[1+\exp\left(\frac{p_{\text{lab}}-1.3}{0.05}\right)\right]^{-1}.$$

2. Medium modified differential cross sections

(1) NN-elastic scattering [10]:

$$\frac{d\sigma_{NN\to NN}(s,t)}{dt} = \frac{1}{(2\pi)^2 s}\left[\frac{(g_{NN}^\sigma)^4}{2(t-m_\sigma^2)^2}(t-4m^{*2})^2 + \frac{(g_{NN}^w)^4}{(t-m_w^2)^2}(2s^2+2st+t^2-8m^{*2}s+8m^{*4}) + \frac{24(g_{NN}^\pi)^4}{(t-m_\pi^2)^2}m^{*4}t^2 - \frac{4(g_{NN}^\sigma g_{NN}^w)^2}{(t-m_\sigma^2)(t-m_w^2)}(2s+t-4m^{*2})m^{*2}\right]. \quad \text{(B4)}$$

The (pseudo)-scalar and vector coupling constants are $g_{NN}^\pi = 7.27$, $g_{NN}^\sigma = 9.4$, and $g_{NN}^w = 10.95$, whereas m^* is the in-medium mass. The Mandelstam variables are given by

$$s = (p+p_2)^2 = [E^*(p)+E^*(p_2)]^2 - (\boldsymbol{p}+\boldsymbol{p}_2)^2, \quad \text{(B5)}$$

$$t = (p-p_3)^3 = \tfrac{1}{2}(s-4m^{*2})(\cos(\theta)-1), \quad \text{(B6)}$$

with θ denoting the scattering angle in the c.m. system. The in-medium single particle energy is given by

$$E^*(p) = \sqrt{p^{*2}+m^{*2}}. \quad \text{(B7)}$$

The formula for the differential cross section of in-medium NN-elastic scattering is extended to all elementary hh collisions by the replacement,

$$s \rightarrow s - (m_1^* - m_2^*)^2 + 4m^{*2}, \tag{B8}$$

where m_1^* and m_2^* denote the effective masses of the incoming hadrons.

(2) $NN \rightarrow N\Delta$ [9]:

$$\frac{d\sigma_{NN\rightarrow N\Delta}(s,t)}{dt} = \frac{8}{(2\pi)^2 s}(g_{NN}^{\pi})^2(g_{\Delta N}^{\pi})^2\left(\frac{(s-m^{*2}-m_\Delta^{*2})^2 - 4m^{*2}m_\Delta^{*2}}{s(s-4m^{*2})}\right)^{1/2} \times [D(s,t)+E(s,t)], \tag{B9}$$

with the direct term,

$$D(s,t) = -\frac{m^{*2}t[(m_\Delta^* + m^*)^2 - t]^2[(m_\Delta^* - m^*)^2 - t]}{6m_\Delta^{*2}(t-m_\pi^2)^2}, \tag{B10}$$

and the exchange term,

$$E(s,t) = -\frac{m^{*2}}{12m_\Delta^{*2}(t-m_\pi^2)(u-m_\pi^2)}\sum_{i=1}^{6} E_i, \tag{B11}$$

where

$$E_1 = m_\Delta^{*2}[(8s-3t)m^{*2}t - 2(s+3t)m^{*4} + 3m^{*6} - 2s^2t + 2t^3],$$

$$E_2 = m_\Delta^{*3}m^*[(2s+t)t - 2(s+t)m^{*2} + 6m^{*4}],$$

$$E_3 = m_\Delta^* m^*[(2s-t)m^{*2}t + (s+3t)m^{*4} + (s+t)st - 3m^{*6}],$$

$$E_4 = m_\Delta^{*5}m^*\lfloor s - t - 3m^{*2}\rfloor + m_\Delta^{*4}[(s-3t)m^{*2} + 2st - t^2],$$

$$E_5 = (s+9t)m^{*6} + (s+6t)(s+t)m^{*2}t - 6(s+2t)m^{*4}t,$$

$$E_6 = -m_\Delta^{*6}m^{*2} - 2m^{*8} - t^2(s+t)^2,$$

with $g_{\Delta N}^{\pi}=15.63$. The definition of s is the same as in Eqs. (B5) and (B8), and

$$t = (p-p_3)^2 = \tfrac{1}{2}(3m^{*2} + m_\Delta^{*2} - s) + 2|\boldsymbol{p}||\boldsymbol{p}_3|\cos(\theta),$$

$$u = (p-p_4)^2 = 3m^{*2} + m_\Delta^{*2} - s - t,$$

$$|\boldsymbol{p}| = \tfrac{1}{2}\sqrt{(s-4m^{*2})},$$

$$|\boldsymbol{p}_3| = \frac{1}{2}\frac{\sqrt{(s-m^{*2}-m_\Delta^{*2})^2 - 4m^{*2}m_\Delta^{*2}}}{\sqrt{s}}.$$

The effects stemming from the finite size of hadrons and a part of the short range correlation is taken into account in Eqs. (B4) and (B9) by introducing a phenomenological form factor at each vertex. For the baryon-baryon-meson vertex the common form,

$$F_{BBM} = \frac{\Lambda_M^2}{\Lambda_M^2 - t}, \tag{B12}$$

is used, where Λ_A is the cut-off mass of the meson A. These cut-off masses are $\Lambda_\pi = 510$ MeV, $\Lambda_\sigma = 1200$ MeV, and $\Lambda_w = 808$ MeV.

Since UrQMD only uses free cross sections and free on-shell particles the effective in-medium quantities E^*, m^*, and m_Δ^* are replaced by the free quantities E, m, and $\langle m_\Delta \rangle$ in actual calculations.

[1] S. Leray *et al.*, Phys. Rev. C **65**, 044621 (2002).
[2] A. Boudard, J. Cugnon, S. Leray, and C. Volant, Phys. Rev. C **66**, 044615 (2002).
[3] J. Cugnon, C. Volant, and S. Vuiller, Nucl. Phys. **A620**, 575 (1997).
[4] A. Engel, E. I. Tanaka, T. Maruyama, A. Ono, and H. Horiuchi, Phys. Rev. C **52**, 3231 (1995).
[5] D. L. Prout *et al.*, Phys. Rev. C **52**, 228 (1995).
[6] W. B. Amian *et al.*, Phys. Rev. C **47**, 1647 (1993).
[7] Kh. Abdel-Waged, A. Abdel-Hafiz, and V. V. Uzhinskii, J. Phys. G **26**, 1105 (2000).
[8] Kh. Abdel-Waged, Phys. Rev. C **67**, 024901 (2003).
[9] G. Mao, Z. Li, Y. Zhuo, and Y. Han, Phys. Rev. C **49**, 3137 (1994).
[10] M. Guangjun, Li Z., Z. Yizhong, H. Yinlu, Y. Ziqiang, and M. Sano, Z. Phys. A **347**, 173 (1994).
[11] B. ter Haar and R. Malfliet, Phys. Rev. C **36**, 1611 (1987).
[12] S. A. Bass *et al.*, Prog. Part. Nucl. Phys. **41**, 225 (1998).
[13] B. Andersson *et al.*, Nucl. Phys. **B281**, 289 (1987).
[14] Kh. Abdel-Waged, Phys. Rev. C **67**, 064610 (2003).
[15] C. Hartnack, R. K. Puri, J. Aichelin, J. Konopka, S. A. Bass, H. Stocker, and W. Greiner, Eur. Phys. J. A **1**, 151 (1998).
[16] V. Weisskopf, Phys. Rev. **52**, 295 (1937); W. A. Friedman and W. G. Lynch, Phys. Rev. C **28**, 16 (1983).
[17] G. Mao, Z. Li, and Y. Zhuo, Phys. Rev. C **53**, 2933 (1996).
[18] R. E. Parel and H. Liechtenstein, Report No. LA-UR-89-3014, Los Alamos National Laboratory, 1989.
[19] D. V. Bugg *et al.*, Phys. Rev. **133**, B1017 (1964).
[20] J. Cugnon, S. Leray, E. Martinez, Y. Patin, and S. Vuiller, Phys. Rev. C **56**, 2431 (1997).
[21] B. E. Bonner, J. E. Simmons, C. R. Newsom, P. J. Riley, G. Glass, J. C. Hiebert, M. Jain, and L. C. Northcliffe, Phys. Rev. C **18**, 1418 (1978).
[22] Particle Data Group, R. M. Barnett *et al.*, Phys. Rev. D **54**, 1 (1996).
[23] J. Cugnon, T. Mizutani, and J. Vandermeulen, Nucl. Phys. **A352**, 505 (1981).